J Mater Sci: Mater Electron (2014) 25:2737–2747
DOI 10.1007/s10854-014-1937-8

Influence of different boron precursors on superconducting and mechanical properties of MgB_2

S. Safran · A. Kılıç · E. Asikuzun · E. Kılıçarslan · O. Ozturk · A. Gencer

Received: 24 February 2014 / Accepted: 7 April 2014 / Published online: 19 April 2014

Abstract The superconducting, structural and mechanical properties of MgB_2 bulk samples have been studied as a function of precursor B powder particle size by means of AC susceptibility, XRD and microhardness measurements, respectively. The in situ processed MgB_2 samples have been prepared by means of conventional solid state reaction method with magnesium powder (99.8 %, 325 mesh) and four different types of boron powders (95.2, >95, 91.9 and 86.7 %) from two sources, Pavezyum and Sigma Aldrich. The XRD measurements showed that the diffraction peaks for our samples belong to the main phase of the MgB_2 diffraction patterns. The highest critical temperature $T_c = 37.7$ K was achieved for the MgB_2 sample which was fabricated by using >95 % purity amorphous boron. Microhardness measurements were performed to investigate the mechanical properties. Load independent hardness, Vickers microhardness, Young's modulus, fracture toughness, and yield strength values were calculated separately for all samples. The results were analyzed by using the Meyer's law, proportional sample resistance model, elastic–plastic deformation model, Hays Kendall approach, and indentation induced cracking (IIC) model. It was found that the IIC model is the most successful model to describe the mechanical properties of our samples.

S. Safran (✉) · A. Kılıç · E. Kılıçarslan · A. Gencer
Department of Physics, Faculty of Science, Ankara University, Tandoğan, 06100 Ankara, Turkey
e-mail: safran@science.ankara.edu.tr; safranserap@gmail.com

S. Safran · A. Kılıç · E. Kılıçarslan · A. Gencer
Center of Excellence for Superconductivity Research, Ankara University, 50. Year Campus, Golbaşı, Ankara, Turkey

E. Asikuzun · O. Ozturk
Department of Physics, Faculty of Arts and Science, Kastamonu University, 37100 Kastamonu, Turkey

1 Introduction

Since the discovery of superconductivity in an intermetallic binary compound MgB_2, a considerable interest has been devoted to understand its ac magnetic response in the superconducting state as well as in its novel properties in the normal state [1–3]. The compound has been found quite attractive because it has a higher critical temperature T_c in comparison to the low-temperature superconductors. Also, MgB_2 has larger superconducting coherence length [1], two different superconducting gaps, no weak links and less anisotropic effects [2, 4] as compared to the high temperature superconductors (HTS).

Another important feature of the MgB_2 is to have very promising T_c and J_c values under the external magnetic field. At this point, the choice of high quality boron has a special importance to enhance the superconducting properties of MgB_2 conductors, especially in applications. Up to the present, a few works were reported on the effects of precursor powders to put forward the role of the boron powder [5–9]. Ribeiro et al. [5] and Zhou et al. [6] reported effects of boron purity and Mg stoichiometry on MgB_2. The influence of the structural form (crystalline and amorphous) and purity of boron precursors on $J_c(H)$ behavior of MgB_2 samples were investigated by Chen et al. [7]. However, a study which examines the effect of purity of precursor boron on the mechanical properties of MgB_2 has not been addressed before.

Hardness is expressed as the resistance against the applied load on a material surface and widely used to determine the production quality of materials in industry. It

is obtained by practical and non-destructive experiments and very useful to determine the success of the process for heat treatment. In particular, understanding the mechanical properties of ceramic superconductors such as elastic modulus, yield strength, fracture toughness and hardness has crucial importance in terms of their usage at applications. In recent years, there is an increasing trend towards the use of MgB_2 superconductors in technological applications [10, 11].

Microhardness or indentation size effect (ISE) is related with the applied test load and in general decreases with increasing the applied load. ISE behavior depends on many factors such as required load to plastic deformation, the elastic recovery, the reaction of the material to elastic/plastic mixed deformation, the size of trace formed during the chipping, the combination of the elastic resistance with the frictional resistance during the chipping of the sample.

The inverse of ISE effect is known as reverse indentation size effect (RISE) and microhardness increases with increasing the applied load. The small indenter effect at low loads, the vibration effect at defective regions of the crystal interface, the loss of energy that occurs as a result of shape change around trace formed during chipping, and the cracks are among the reasons of the RISE behavior. But this phenomenon has not been still fully explained [12].

The aim of this study is to investigate effects of precursor boron purity on the superconducting and mechanical properties for MgB_2. In the present work, we report on the results obtained from two set of MgB_2 samples fabricated by two different milling procedures. In each set, there are four samples prepared by different amorphous boron precursor powder purity. Hence we studied effects of the purity of precursor boron powder and milling procedure on mechanical and superconducting properties of MgB_2 bulk samples.

2 Experimental details

MgB_2 powders were prepared by in situ solid state reaction method with a mixture of Mg powder (99.8 % purity) and four different amorphous boron precursor powders with nominal purities of 95.2, 91.9 and 86.7 % from *PAVEZYUM*, which is a native supplier, and >95 % from *SIGMA-ALDRICH*. The particle sizes of boron precursor powder are 0.8 and $\leq$1 μm for native and Sigma-Aldrich, respectively. We do not have any information about how to determine the particle sizes of boron precursors. The Mg and B powders were ball-milled separately. The milling procedure was maintained in a stainless-steel jar together with stainless-steel balls. The powder and ball weight ratio was chosen to be 1:11. The Mg powder was milled for 1:11 h with a rotating speed of 111 rpm. B powder was milled for 5 and 11 h with a rotating speed of 151 rpm. Then the mixture of B and Mg, in a nominal atomic composition of Mg + 2B, was mixed for 1:11 h with a rotating speed of 111 rpm. However, we have ignored the contribution of natural Mg in the original B powder. The mixture powder was then pressed into pellets about 11.4 mm long and 2.9 mm wide using a hydraulic press with an applied load of 5 tones. All the samples were then placed into a stainless steel tube and sintered at 800 °C for 1 h under 10 bar high purity Argon atmosphere. The heating rate was 5 °C/min and the samples quenched to air for cooling process. The details about the preparation of samples are given in Fig. 1.

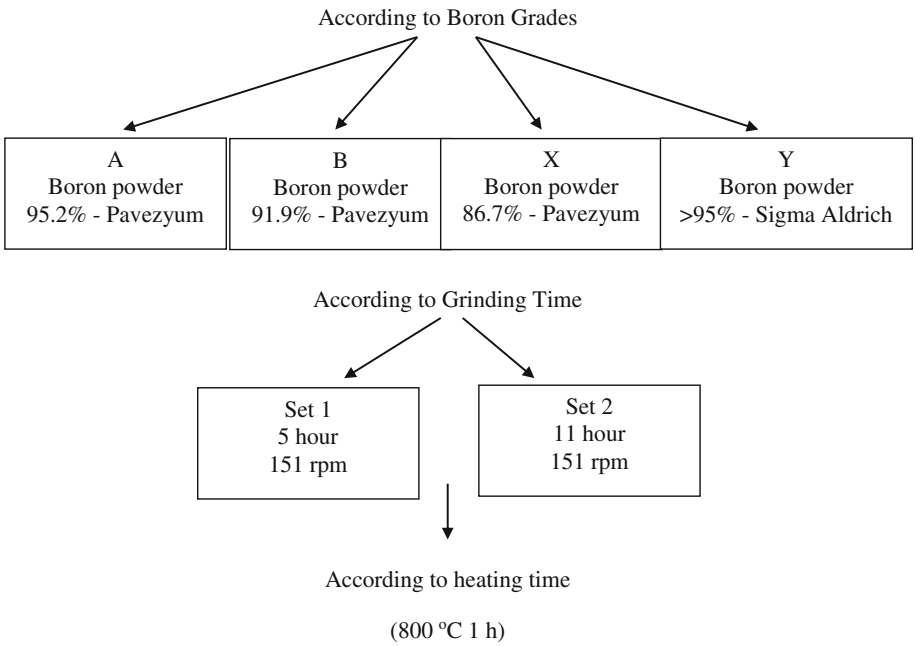

Fig. 1 The schematic procedure of preparation

Our samples have been investigated by means of XRD, AC susceptibility and microhardness measurements. Rigaku D/Max-IIIC diffractometer (XRD) was used with CuK_α radiation to determine XRD spectra of all the samples. The susceptibility measurements were carried out by a commercial Lake Share 7130-model ac susceptometer employing a mutual inductance coil system with a closed cycle refrigerator. Vickers microhardness measurements are conducted at room temperature in air by using a digital microhardness tester (SHIMADZU HVM-2) to obtain information about the physical and the mechanical properties of the bulk MgB_2 samples prepared at different conditions. A rigid Vickers pyramidal indenter is applied for 10 s using different load in the range from 0.245 to 2.940 N and the diagonals of indentation are measured with an accuracy of ±0.1 μm. The Vickers microhardness measurements are performed with an average of 10 readings at different locations of sample surfaces to obtain reasonable mean values for each applied load. The microhardness measurements are analyzed by means of various models.

3 Results and discussion

3.1 Structural and superconducting properties

Figure 2a, b shows the XRD patterns of the two set of MgB_2 samples obtained from various purities of precursor boron powders. The X-ray diffraction peaks of the superconducting samples showed sharp peaks of MgB_2 phase with only small fraction of MgO and boride peaks. The intensity of these impurity phases also increased when the purity of boron precursor powder was decreased. The patterns indicated that there is no residual Mg powder inside since the heat treatment was done at sufficiently high temperatures. Some boride peaks (MgB_4, MgB_{12}) appeared in our samples and it is an evident that some Mg was evaporated during the heat treatment process. Another observation from the XRD patterns is that there is no peak shifting with increasing of precursor boron purity as shown in Fig. 2. However, there is a small broadening at the main peak with increasing the milling time for boron precursor. According to Scherrer's formula, $d = K\lambda/\beta\cos(\theta)$, where d is the mean crystalline size, K is a grain shape dependent constant (0.9), λ is the wavelength of the incident beam, θ is a Bragg reflection angle and β is the full width half maximum (FWHM). The FWHM value of the (101) main peaks for our different samples is shown in Table 1. As seen from the Table 1, FWHM is proportional to the milling time and when the milling time increases, the grain size is decreased.

Plots of real (χ') and imaginary (χ'') components of AC susceptibility as a function of temperature for Set 1 and Set 2 samples at applied AC field amplitudes H_{ac}, ranging from 80 to 1,280 A/m at a frequency $f = 125$ Hz were given at Fig. 3a, b, respectively. Fundamental susceptibility shows a typical single-step transition. This single step transition, reflecting the flux penetration into the bulk of MgB_2, indicates the presence of a strong coupling between the

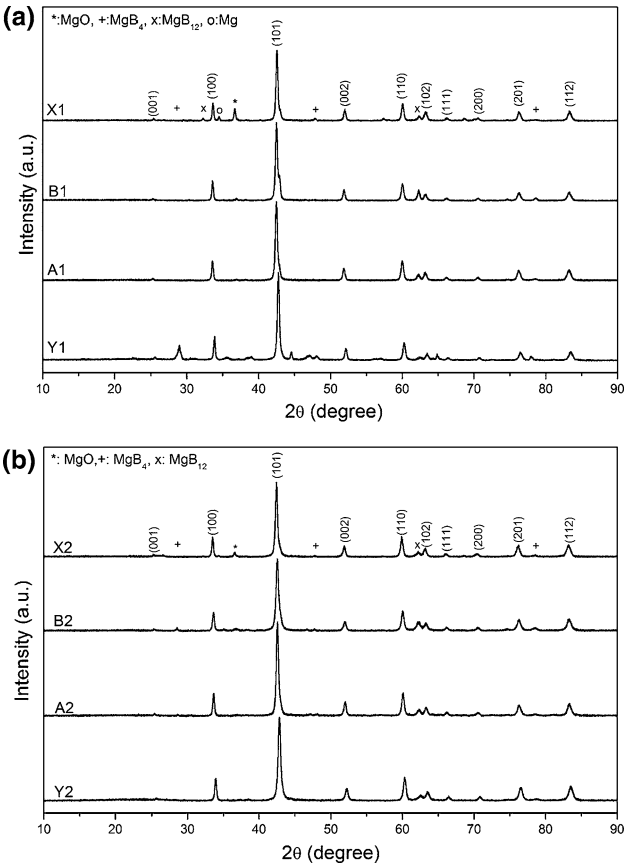

Fig. 2 **a** X-ray diffraction patterns of MgB_2 samples of set 1. **b** X-ray diffraction patterns of MgB_2 samples of set 2

Table 1 Microstructure and superconducting parameters of samples

Sample name	Source	Boron purity (%)	2θ of (101) main peak (°)	FWHM of (101) peak	T_c^{onset} (K)	ΔT_c (K)
Y1	Sigma-Aldrich	>95	42.73	0.345	37.7	0.9
A1	Pavezyum	95.2	42.48	0.368	36.6	1.3
B1	Pavezyum	91.9	42.49	0.348	36.6	1.1
X1	Pavezyum	86.7	42.57	0.335	36.7	0.9
Y2	Sigma-Aldrich	>95	42.84	0.445	37.6	0.9
A2	Pavezyum	95.2	42.55	0.385	36.7	0.8
B2	Pavezyum	91.9	42.53	0.467	36.5	1.4
X2	Pavezyum	86.7	42.41	0.380	36.9	1.2

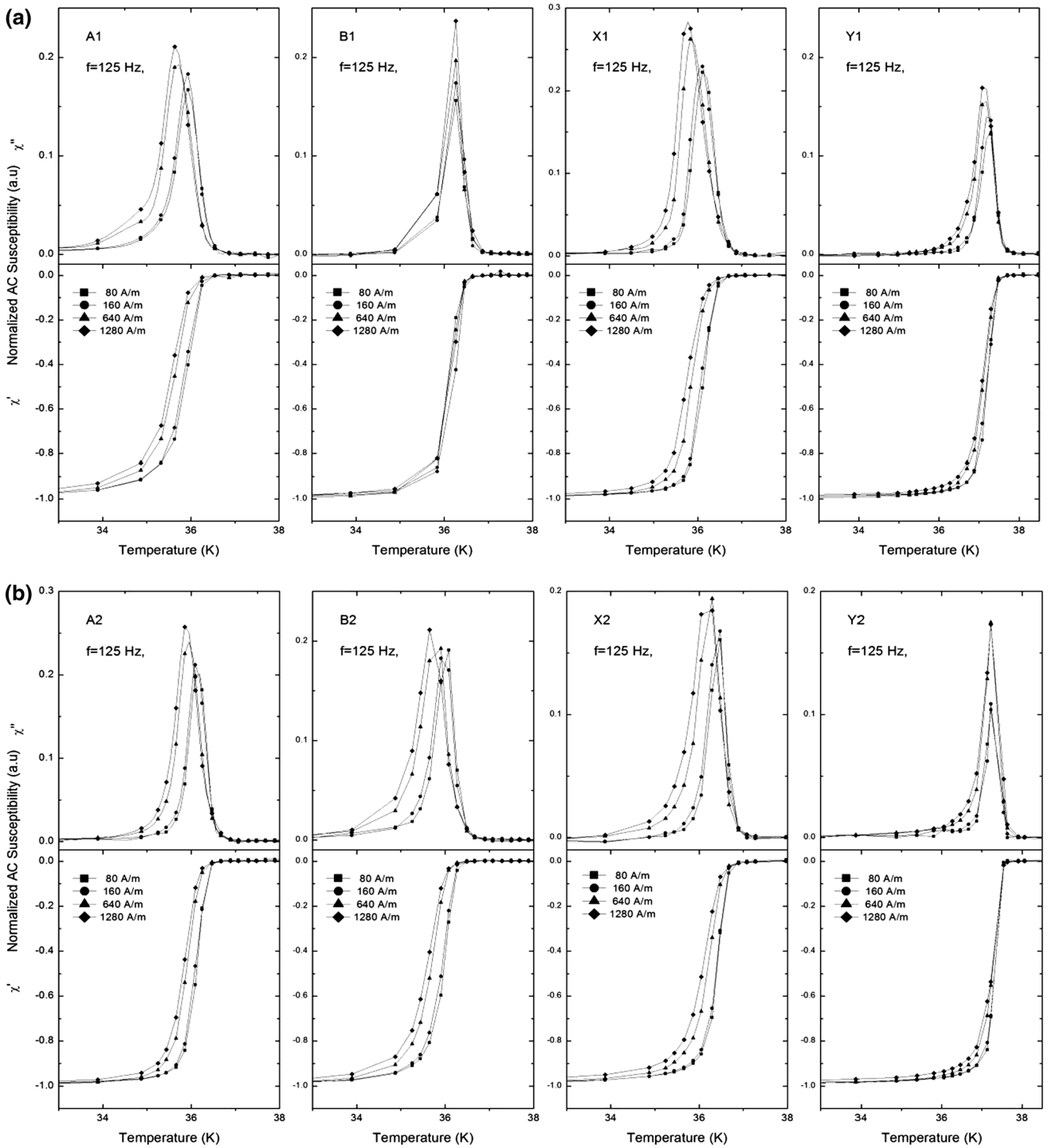

Fig. 3 **a** Plot of real (χ') and imaginary (χ'') components of AC susceptibility as a function of temperature of MgB_2 samples of set 1 taken at applied AC field amplitudes H, ranging from 80 to 1,280 A/m at a frequency f = 125 Hz. **b** Plot of real (χ') and imaginary (χ'') components of AC susceptibility as a function of temperature of MgB_2 samples of set 2 taken at applied AC field amplitudes H, ranging from 80 to 1,280 A/m at a frequency f = 125 Hz

grains of MgB_2. It was found that the influence of the field strength is negligible for B1 sample in Set 1. When H_{ac} is increased from 80 to 1,280 A/m, the peak height in χ'' increased without any change at the peak position. Similar behavior is also observed for Y2 sample in Set 2. However, for the other samples, when H_{ac} is increased from 80 to 1,280 A/m, the peak height in χ'' was also increased and the peak moved to lower temperatures slightly. These results

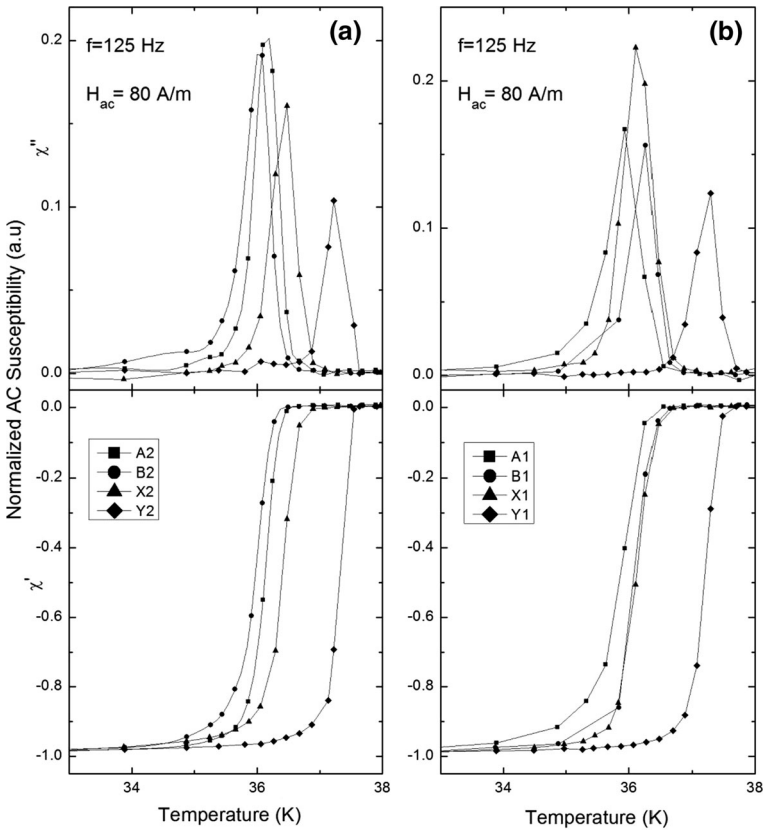

Fig. 4 The temperature dependence of normalized ac susceptibility of **a** Set 2 and **b** Set 1 samples

suggested that B1 and Y2 samples have a better intergranular coupling between grains.

In Fig. 4a, b, we have plotted the normalized ac susceptibility curves as a function of temperature at $H_{ac} = 80$ A/m, frequency $f = 125$ Hz. T_c values and transition width ΔT of the samples were determined from Fig. 4 by using an onset criterion and 10–90 % criterion, respectively. We observed that T_c was decreased from 37.7 to 36.5 K with changing of the purity of boron powder, but there is no systematic behavior. It was expected that the higher boron purity would cause higher T_c values but the non-systematic behaviour revealed the importance of impurity level in the boron precursor on T_c. When we compare the two set of samples, there is minor effect of milling time on the T_c as shown in Table 1. On the other hand, a sharp diamagnetic transition in fundamental susceptibility shows that the desired homogeneity was achieved for the samples.

3.2 Mechanical properties

3.2.1 Vickers microhardness measurements and models

Vickers microhardness measurements were performed for characterization of mechanical properties of materials. The measurements were taken using the *Shimadzu HVM-2* model microhardness device at room temperature. Vickers indenter that is made from diamond with a shape of square pyramid suspended on a surface of the material under different loads (0.245, 0.490, 0.980, 1.960 and 2.940 N) and diagonal lengths of trace were measured. 10 measurements were taken for each load value and d_1 and d_2 diagonal lengths were calculated with their average. Vickers microhardness values

$$H_v = 1854.4 \frac{P}{\left(\frac{d_1+d_2}{2}\right)^2} \quad (1)$$

were calculated by Eq. 1. Where P is the applied load, d_1 and d_2 are diagonal lengths of trace occurs after the tip removed. Elastic modulus (E), Yield strength (Y) and Fracture toughness (K_{IC}) of materials from obtained hardness values (H_v)

$$E = 81,9635 H_v \quad (2)$$

$$Y \approx H_v/3 \quad (3)$$

$$K_{IC} = \sqrt{2Ea} \quad (4)$$

were calculated other mechanical parameters by the formula given above.

Vickers hardness measurement takes longer time than other hardness measurements but it is one of the most sensitive hardness measurement methods. It has one of the most suitable tip that can be used as an alternative to Berkovich tip especially in the investigation of micro-and nano-sized hardness.

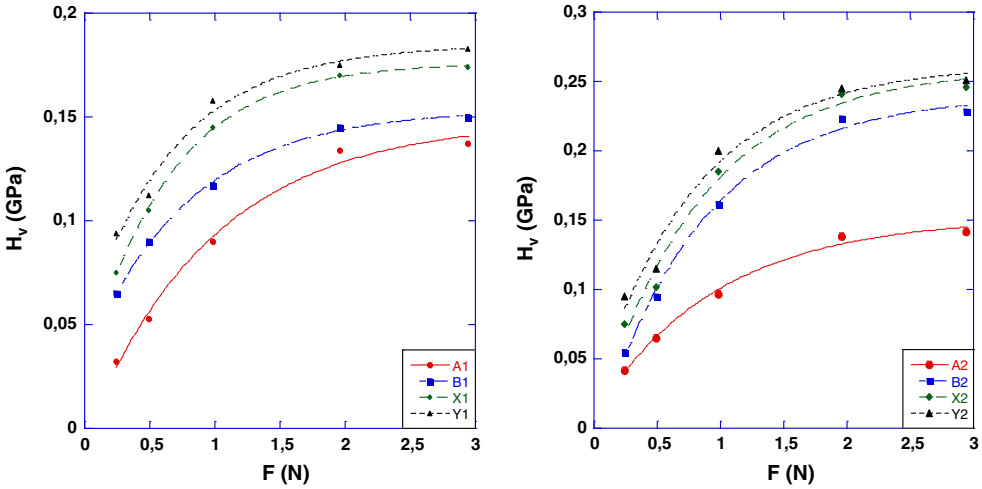

Fig. 5 The variations of microhardness with load for the samples

Figure 5 shows the variation of Vickers hardness values as a function of the applied load. Here, it can be easily seen that microhardness values of all samples depend on applied indenter load, regardless of different purity B powders (95.2 %—Alfa Aesar, 91.9 %—Alfa Aesar, 86.7 %—Alfa Aesar, and >95 %—Sigma Aldrich) and different grinding times (5–11 h). Such a relation between the hardness values and the applied loads is considered as reverse indentation size effect (RISE) or indentation size effect (ISE). RISE is evidently seen on all samples and the microhardness values increase with the enhancement of the applied load (Table 2).

Up to date, several models have been suggested to explain the ISE and RISE such as the Meyer Law, proportional sample resistance (PSR) model, elastic/plastic deformation (EPD) model, Hays–Kendall (HK) approach and indentation induced cracking (IIC) model. Analyses on these models are given below [13].

Microhardness increased with decreasing the purity of Pavezyum brand B powder. When Sigma Aldrich (>95 %) brand B powder is used, microhardness increased to its highest value. When the grinding time is considered, it can be said that greater hardness value was obtained in the samples milled for 11 h.

The saturation level for microhardness values was about 2 N for the samples. This means that there is no significant change in microhardness of the samples above that level.

3.2.2 *Analysis according to Meyer law*

Meyer's law is used to determine ISE or RISE of the material and the most basic hardness model. This law is expressed by a simple relation between applied load P and diagonal length d:

$$P = Ad^n \tag{5}$$

n exponent, obtained from the slope of *InP-Ind* graph, determines ISE or RISE behavior of the material (Fig. 6). RISE behavior occurs when the n_K value is greater than 2, and if the n_K value is less than 2, ISE behavior is obtained. When n_K is equal 2, hardness is load independent and this gives the Kick's law [14–16].

The slope of the graph in Fig. 6 gives n, and the vertical intercept is A. For all sample, we found that Meyer number is greater than 2 and load dependent displacement has RISE behavior. The results obtained from the graph are summarized in Table 3.

3.2.3 *Analysis according to proportional sample resistance (PSR) model*

This method is developed by Li and Bradt [17], the relationship between P and d is given by the Eq. 6.

$$P = ad + bd^2 \tag{6}$$

where a is the surface energy and b is a parameter in order to calculate the real hardness value. a and b are calculated from Fig. 7. Load-independent hardness value in PSR model is calculated from Eq. 7.

$$H_{PSR} = 1854.4b \tag{7}$$

Calculated values of a, b and H_{PSR} are given in Table 4. Here, a is negative for all samples. This confirms that there is only plastic deformation in all samples, that is, RISE behavior. When we compare the microhardness values of the samples calculated from PSR model [18–20], we found that these values are far from the values of the plateau region obtained from Fig. 5. This model is used for the hardness analysis of the materials having ISE behavior thus quite far from the plateau region of hardness values is an expected result.

3.2.4 *Analysis according to elastic/plastic deformation (EPD) model*

According to Bull et al. [21, 22], the dependence of indentation size on the applied load is given as;

Table 2 The calculated load dependent H_v, E, Y, and K_{IC} values for the samples

Samples	P(N)	H_v (GPa)	d_{ort} (μm)	E (GPa)	Y (GPa)	K_{ic} (Pa/m$^{1/2}$)
A1	0.245	0.032	119.27	2.622	0.010	−29.504
	0.490	0.053	130.38	4.344	0.017	−37.976
	0.980	0.090	142.88	7.376	0.030	−49.486
	1.960	0.134	164.41	10.98	0.044	−60.377
	2.940	0.137	200.68	11.22	0.045	−61.033
B1	0.245	0.065	83.66	5.327	0.021	−27.074
	0.490	0.090	101.03	7.376	0.030	−31.858
	0.980	0.117	124.72	9.589	0.039	−36.324
	1.960	0.145	158.51	11.88	0.048	40.431
	2.940	0.150	191.70	12.29	0.050	−41.123
X1	0.245	0.075	78.26	6.147	0.025	−30.386
	0.490	0.105	93.54	8.606	0.035	−35.953
	0.980	0.145	112.09	11.88	0.048	−42.242
	1.960	0.170	145.80	13.93	0.056	−45.742
	2.940	0.174	176.69	14.26	0.058	46.280
Y1	0.245	0.094	70.00	7.704	0.031	−30.329
	0.490	0.112	90.36	9.179	0.037	−33.105
	0.980	0.158	107.37	12.95	0.052	−39.322
	1.960	0.175	143.73	14.34	0.058	−41.379
	2.940	0.183	173.20	14.99	0.061	−42.306
A2	0.245	0.042	103.24	3.442	0.014	−36.128
	0.490	0.075	110.67	6.147	0.025	−48.280
	0.980	0.122	122.78	9.999	0.040	−61.576
	1.960	0.178	143.63	14.59	0.059	−74.381
	2.940	0.182	172.87	14.91	0.060	−75.192
B2	0.245	0.055	90.97	4.508	0.018	−43.689
	0.490	0.095	98.02	7.786	0.031	−57.416
	0.980	0.152	109.32	12.45	0.050	−72.604
	1.960	0.223	127.69	18.27	0.074	−87.952
	2.940	0.233	153.36	19.09	0.077	−89.904
X2	0.245	0.075	78.26	6.147	0.025	−46.542
	0.490	0.105	93.54	8.606	0.035	−55.070
	0.980	0.165	105.52	13.52	0.055	−69.025
	1.960	0.241	122.65	19.75	0.080	−83.426
	2.940	0.250	148.12	20.49	0.083	−84.975
Y2	0.245	0.083	74.62	6.803	0.027	−47.510
	0.490	0.118	88.19	9.671	0.039	−56.647
	0.980	0.182	100.00	14.91	0.060	−70.336
	1.960	0.255	119.61	20.90	0.085	−83.274
	2.940	0.264	143.88	21.63	0.088	−84.716

$$P = B(d_p + d_e)^2 \tag{8}$$

where B is the load independent hardness constant, and d_e (elastic deformation) is related to the d_p (plastic deformation). The values of d_e and B are calculated by the variation

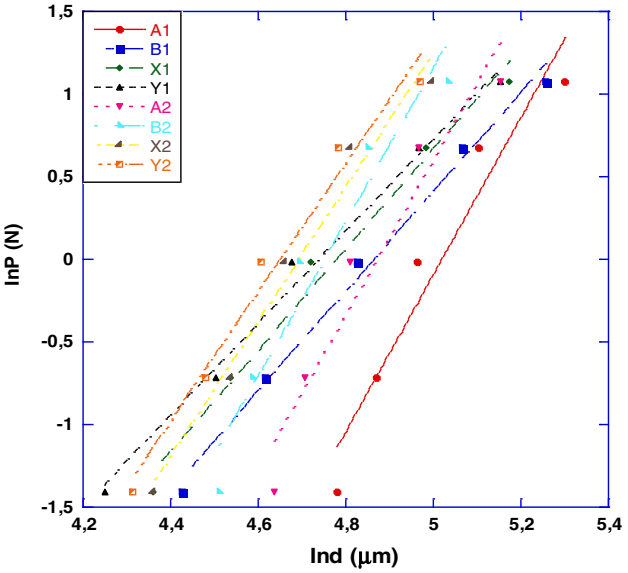

Fig. 6 Variation of applied load *lnP* with diagonal *lnd* for the samples

Table 3 Best-fit results of experimental data according to Meyer's law

Samples	Slope n	lnA (GPa)
A1	4.68	−22.84
B1	4.65	−22.13
X1	4.06	−19.09
Y1	3.89	−18.11
A2	4.75	−23.87
B2	3.01	−14.65
X2	3.04	−14.57
Y2	2.78	−13.19

of the square root of applied load ($P^{1/2}$) with the indentation size (d) as depicted in Fig. 8. The load independent microhardness with this model is calculated from;

$$H_{EPD} = 1854.4B \tag{9}$$

In Table 5, all the obtained values are listed. It is seen from the table that the value of d_e is found to be negative for all samples. This means that there is not any trace for the elastic deformation in the material and confirms that the plastic deformations are only produced in the samples under the applied load. As can be seen from the Table 5, load-independent hardness values that were calculated from the EDP model are so far from the results in the plateau region. Therefore, this model is not reasonable for the hardness analysis of the materials.

3.2.5 Analysis according to Hays–Kendall (HK) approach

Hays and Kendall [23] suggested that there exists a minimum applied test load W necessary to initiate plastic

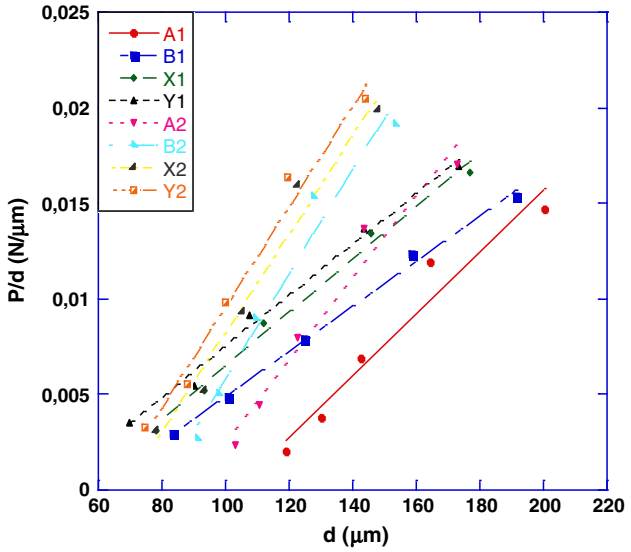

Fig. 7 Plots of *P/d* versus *d* for the samples

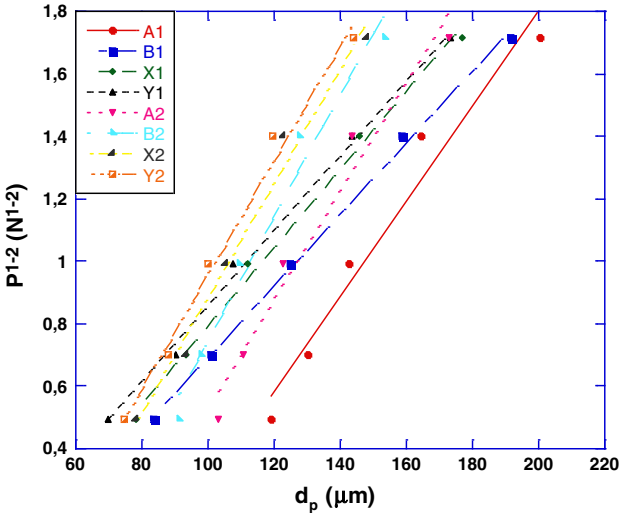

Fig. 8 Plots of diagonal length versus square root of applied loads for the samples

Table 4 Best-fit results of experimental data according to *PSR* model

Samples	a × 10^{-3} (N)	b × 10^{-5} (N/μm)	H_{PSR} (GPa)	H_v (GPa)
A1	−16.60	16.13	0.299	0.134–0.137
B1	−6.88	11.78	0.218	0.145–0.150
X1	−7.51	13.98	0.259	0.170–0.174
Y1	−5.97	13.43	0.249	0.175–0.183
A2	−18.96	21.47	0.398	0.178–0.182
B2	−21.17	27.11	0.502	0.223–0.233
X2	−17.62	25.83	0.478	0.241–0.250
Y2	−16.59	26.30	0.487	0.255–0.264

Table 5 Best-fit results of experimental data according to *EPD* model

Samples	$B^{1/2}$ (N/mm^2)	d_e (mm)	H_{EPD} (GPa)	H_v (GPa)
A1	0.015	−1.24	0.417	0.134–0.137
B1	0.011	−0.44	0.224	0.145–0.150
X1	0.013	−0.45	0.313	0.170–0.174
Y1	0.012	−0.34	0.267	0.175–0.183
A2	0.017	−1.22	0.535	0.178–0.182
B2	0.019	−1.21	0.669	0.223–0.233
X2	0.018	−0.95	0.600	0.241–0.250
Y2	0.018	−0.86	0.600	0.255–0.264

deformation in which the only elastic deformation occurs (Fig. 9)

$$P_{eff} = P_{\max} - W = Kd^2 \quad (10)$$

where K indicates a constant related to the applied test load W which shows the minimum load necessary to initiate the permanent deformation. The load independent W and K values are shown in Table 6.

It is seen from the Table 6, the W values are negative for all the samples, the RISE behavior. A negative W value results from dominant characterization of the plastic deformation in the system [24]. If W is positive, it can be said that the applied load is high enough to produce the elastic (reversible) deformation as well as the plastic (irreversible) deformation in the materials. In this case, the material shows ISE behavior. According to this result, we did not observe elastic deformation on the samples. Only plastic deformation was observed on all the samples exhibiting the RISE behavior.

The hardness value from HK model is so far from the hardness value in the plateau region. In general, it is pointed out that the load independent hardness value should be close to the value of the plateau region [25, 26]. For this reason, Hays–Kendall model is not an appropriate model in the analysis of microhardness and determining the mechanical properties of the samples which shows the RISE behavior.

3.2.6 *Analysis according to indentation induced cracking (IIC) model*

IIC model developed by Li and Bradt explains to RISE behavior [27]. According to this model, the applied test load is equilibrated by the total sample resistance in maximum depth. This resistance is composed of four components.

(a) Shift of the indenter or sample at the interface
(b) Elastic Deformation

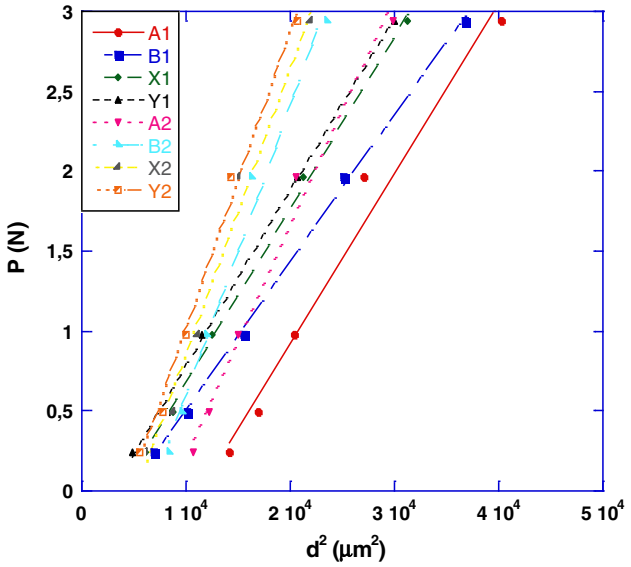

Fig. 9 Applied load versus the square of the impression semi-diagonal length for the samples

Table 6 Best-fit results of experimental data according to *HK* model

Samples	K × 10^{-5}	W_{HK} (N)	H_{HK} (GPa)	H_v (GPa)
A1	10.00	−1.20	0.185	0.134–0.137
B1	9.22	−0.42	0.170	0.145–0.150
X1	10.88	−0.41	0.201	0.170–0.174
Y1	10.92	−0.32	0.202	0.175–0.183
A2	14.22	−1.19	0.263	0.178–0.182
B2	18.00	−1.18	0.333	0.223–0.233
X2	17.98	−0.94	0.334	0.241–0.250
Y2	18.56	−0.84	0.344	0.255–0.264

(c) Plastic Deformation
(d) Cracks of sample

The friction (sliding) and elastic effects lead to normal ISE behavior according to Li and Bradt, whilst indentation cracking causes the RISE behavior. Li and Bradt had reported to the importance of elastic and friction effects in the PSR model. In this model, calculated hardness value using Vickers diamond tip,

$$H_v = \lambda_1 K_1 \left(\frac{P}{d^2}\right) + K_2 \left(\frac{P^{5/3}}{d^3}\right) \tag{11}$$

is given by the equation. Where d is the diameter of trace, λ_1, K_1 and K_2 are constants. K_2 depends on the applied load and K_1 depends on the indenter geometry.

If the equations $H_v = K_1(P/d^2)$, $\lambda_1 = 1$ and $K_2(P^{5/3}/d^3) = 0$ are satisfied, the materials are ideal plastic materials. If the equations are in these forms of $H_v = K_2\ (P^{5/3}/d^3)$ and $\lambda_1 = 0$, material is perfect brittle solid. Then the only second term in the Eq. 11 is used when the material is brittle. In this study, the elastic deformation was not observed in our samples. These materials have more brittleness and the most appropriate hardness results are calculated using the Eq. 12.

$$H_v = K\left(\frac{P^{5/3}}{d^3}\right)^m \tag{12}$$

K and m values are load independent constants and they are obtained from the $In(Hv)$-$In(P^{5/3}/d^3)$ graph (Fig. 10). Power m is used for the determination of ISE behavior. If m is greater than 0.6 the material has a normal ISE behavior. But if m is less than 0.6 it has a RISE behavior [12, 28].

In the hardness analysis, IIC model was found as the most suitable one for all the samples which has no elastic

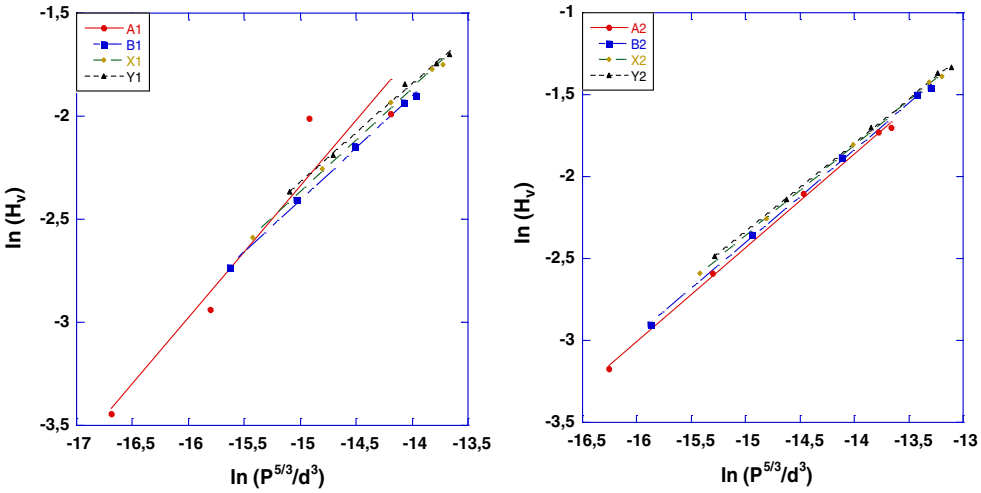

Fig. 10 Variation of $\ln H_V$ with $\ln (P^{5/3}/d^3)$ according to *IIC* model for all samples

Table 7 Best-fit results of experimental data according to *IIC* model

Samples	m	$K \times 10^4$ ($N^{(3-5m)/3}/\mu m^{(2-3m)}$)	H_{IIC} (GPa)	H_V (plateau region) (GPa)
A1	0.63	0.1352	0.115	0.134–0.137
B1	0.51	0.0181	0.108	0.145–0.150
X1	0.50	0.0174	0.136	0.170–0.174
Y1	0.47	0.0127	0.160	0.175–0.183
A2	0.57	0.0454	0.119	0.178–0.182
B2	0.56	0.0428	0.159	0.223–0.233
X2	0.55	0.0340	0.157	0.241–0.250
Y2	0.54	0.0317	0.179	0.255–0.264

Table 8 The results of load dependent Vickers microhardness at the plateau region and load independent hardness values calculated using *PSR*, *EPD*, *HK* and *IIC* models

Samples	H_{PSR} (GPa)	H_{EPD} (GPa)	H_{HK} (GPa)	H_{IIC} (GPa)	H_V (GPa) (in plateau region)
A1	0.299	0.417	0.185	0.115	0.134–0.137
B1	0.218	0.224	0.170	0.108	0.145–0.150
X1	0.259	0.313	0.201	0.136	0.170–0.174
Y1	0.249	0.267	0.202	0.160	0.175–0.183
A2	0.398	0.535	0.263	0.119	0.178–0.182
B2	0.502	0.669	0.333	0.159	0.223–0.233
X2	0.478	0.600	0.334	0.157	0.241–0.250
Y2	0.487	0.600	0.344	0.179	0.255–0.264

deformation. Power m is obtained from slope of the graph for the samples having values that change between 0.63 and 0.47 (Table 7). As mentioned above, the sample shows normal ISE for $m > 0.6$ and RISE behavior $m < 0.6$. When the power m values are considered, we can say that all the samples show RISE behavior.

As a result, when all models mentioned above are applied on the samples, since the materials show the RISE behavior it is concluded that IIC model is used in the literature to explain this behavior is the most appropriate. These results are summarized in Table 8.

4 Conclusion

MgB_2 powders were prepared by in situ solid state reaction method with a mixture of Mg powder (99.8 % purity) and four different amorphous boron precursor powders. XRD and AC susceptibility measurements have been performed to investigate the structural and superconducting properties, respectively. To determine the mechanical properties, Vickers microhardness measurements were applied. The results of the microhardness measurements were analyzed by using Meyer's law, PSR, EPD, IIC models, and Hays–Kendall (HK) approach. The following results are obtained;

- The higher precursor boron powder purity causes the formation of lower impurity phases.
- When the milling time increases, the grain size decreases.
- Different purity of boron powder affects the transition temperature.
- There is a minor deviation in the transition temperature with increasing milling time.
- Microhardness value increased with decreasing the purity of Pavezyum brand B powder. When Sigma Aldrich (>95 %) brand B powder was used, the microhardness reached its highest value. When the grinding time is considered, it can be said that greater hardness value is obtained for the samples milled for 11 h.
- Vickers microhardness values increased with increasing the applied load. The load dependence showed that RISE has an influence on the samples.
- Elastic modulus, yield strength, and fracture toughness values changed with microhardness values for load dependent case. The load dependent microhardness, elastic modulus, yield strength and fracture toughness were calculated by means of the Eqs. (1)–(4).
- The results of the microhardness measurements were analyzed by employing Meyer's law, PSR, EDP, IIC models, and Hays–Kendall approach. IIC model was found to be the best model describing the microhardness of our samples.

References

1. J. Nagamatsu, N. Nakagawa, T. Muranaka, Y. Zenitani, J. Akimitsu, Nature **410**, 63 (2001)
2. D.C. Larbalestier, L.D. Cooley, M.O. Rikel, A.A. Polyanskii, J. Jiang, S. Patnaik, X.Y. Cai, D.M. Feldmann, A. Gurevich, A.A. Squitieri, M.T. Naus, C.B. Eom, E.E. Hellstrom, R.J. Cava, K.A. Regan, N. Rogado, M.A. Hayward, T. He, J.S. Slusky, P. Khalifah, K. Inumaru, M. Haas, Nature **410**, 186 (2001)
3. E.G. Killian, R.B. Kaner, Chem. Mater. **8**, 333 (1996)
4. M. Kambara, N. Haribabu, E.S. Sadki, J.R. Cooper, H. Minami, D.A. Cardwell, A.M. Campbell, I.H. Inoue, Supercond. Sci. Technol. **14**, L5 (2001)
5. R.A. Ribeiro, S.L. Bud'ko, C. Petrovic, P.C. Canfield, Phys. C **385**, 16 (2003)
6. S. Zhou, A.V. Pan, J. Horvat, M. Qin, H.K. Liu, Supercond. Sci. Technol. **17**, S528 (2004)
7. S.K. Chen, K.A. Yates, M.G. Blamire, J.L. MacManus-Driscoll, Supercond. Sci. Technol. **18**, 1473 (2005)
8. X. Xu, M.J. Qin, K. Konstantinov, D.I.D. Santos, W.K. Yeoh, J.H. Kim, S.X. Dou, Supercond. Sci. Technol. **19**, 466 (2006)
9. W. Häßler, B. Birajdar, W. Gruner, M. Herrmann, O. Perner, C. Rodig, M. Schubert, B. Holzapfel, O. Eibl, L. Schultz, Supercond. Sci. Technol. **19**, 512 (2006)

10. M. Dogruer, O. Gorur, Y. Zalaoglu, O. Ozturk, G. Yildirim, A. Varilci, C. Terzioglu, J. Mater. Sci.: Mater. Electron. **24**, 352 (2013)
11. M. Dogruer, Y. Zalaoglu, O. Gorur, O. Ozturk, G. Yildirim, A. Varilci, E. Yucel, C. Terzioglu, J. Mater. Sci.: Mater. Electron. **24**, 776 (2013)
12. K. Sangwal, Mater. Chem. Phys. **63**, 145 (2000)
13. L. Arda, O. Ozturk, E. Asikuzun, S. Ataoglu, Powder Technol. **235**, 479 (2013)
14. O. Ozturk, H.A. Cetinkara, E. Asikuzun, M. Akdogan, M. Yilmazlar, C. Terzioglu, J. Mater. Sci.: Mater. Electron. **22**, 1501 (2011)
15. E. Asikuzun, O. Ozturk, H.A. Cetinkara, G. Yildirim, A. Varilci, M. Yılmazlar, C. Terzioglu, J. Mater. Sci.: Mater. Electron. **23**, 1001 (2012)
16. O. Ozturk, E. Asikuzun, G. Yildirim, J. Mater. Sci.: Mater. Electron. **24**, 1274 (2012)
17. H. Li, R.C. Bradt, J. Mater. Sci. **28**, 917 (1993)
18. J.B. Quinn, V.D. Quinn, J. Mater. Sci. **32**, 4331 (1997)
19. M. Yilmazlar, O. Ozturk, O. Gorur, I. Belenli, C. Terzioglu, Supercond. Sci. Technol. **20**, 365 (2007)
20. M. Yılmazlar, H.A. Cetinkara, M. Nursoy, O. Ozturk, C. Terzioglu, Phys. C **442**, 101 (2006)
21. S.J. Bull, T.F. Page, E.H. Yoffe, Phil. Mag. Lett. **59**, 281 (1989)
22. G.P. Upit, S.A. Varchenya, Phys. Status Solidi A **17**, 831 (1966)
23. C. Hays, E.G. Kendall, Metallurgy **6**, 275 (1973)
24. R. Awad, A.I. Abou-Aly, M. Kamal, M. Anas, J. Supercond. Novel Magn. **24**, 1947 (2011)
25. J. Gong, Z. Zhao, Z. Guan, H. Miao, J. Eur. Ceram. Soc. **20**, 1895 (2000)
26. Z.J. Peng, J.H. Gong, H.Z. Miao, J. Eur. Ceram. Soc. **24**, 2193 (2004)
27. H. Li, R.C. Bradt, J. Mater. Sci. **31**, 1065 (1996)
28. R. Awad, A.I. Abou-Aly, M. Kamal, M. Anas, J. Supercond. Nov. Magn. **24**, 1947 (2011)